Snow failure modes under mixed loading

Tijan Mede, Guillaume Chambon, Pascal Hagenmuller, François Nicot

AGU100 ADVANCING EARTH AND SPACE SCIENCE

Geophysical Research Letters

RESEARCH LETTER
10.1029/2018GL080637

Key Points:
- Large-strain responses of microCT-reconstructed snow samples are simulated under shear and normal loading
- Three distinct failure modes are identified, and sample collapse is analyzed
- Simulated results appear qualitatively similar for different snow types

Correspondence to:
T. Mede,
tijan.mede@irstea.fr

Citation:
Mede, T., Chambon, G., Hagenmuller, P., & Nicot, F. (2018). Snow failure modes under mixed loading. *Geophysical Research Letters*, *45*, 13,351–13,358. https://doi.org/10.1029/2018GL080637

Received 25 SEP 2018
Accepted 7 DEC 2018
Accepted article online 12 DEC 2018
Published online 26 DEC 2018

Snow Failure Modes Under Mixed Loading

Tijan Mede[1], Guillaume Chambon[1], Pascal Hagenmuller[2], and François Nicot[1]

[1]Université Grenoble Alpes, Irstea, UR ETGR, Grenoble, France, [2]Université Grenoble Alpes, Université de Toulouse, Météo-France, CNRS, CNRM, Centre d'Etudes de la Neige, Grenoble, France

Abstract The mechanical response of snow to mixed-mode shear and normal loading is the key ingredient for snow avalanche modeling and strongly depends on microstructural characteristics. A discrete element numerical model was developed, which enables the simulation of large-strain response of snow samples directly described by their full microstructure obtained through X-ray microtomography. The model offers new insights into the failure mechanism as well as postfailure response of snow in mixed-mode loading. Three distinct failure modes are identified, depending on the value of applied normal stress. Above a certain threshold normal stress, the failure is characterized by a structural collapse that decomposes the snow sample into a set of cohesionless grains. It is shown that the collapse is a dynamic process, which, once initiated, develops independently of shearing. This behavior was consistently observed for different snow types, including faceted crystals typically composing weak layers.

Plain Language Summary Snow avalanches are a major natural hazard in mountainous areas due to their destructive power and seemingly unpredictable occurrence. The increase in computing power and development of computation tools in the recent years have opened the prospect of using large-scale computer simulations in order to better understand these catastrophic events. The reliability of a snow avalanche simulation heavily depends on the accuracy of constitutive models used to describe the mechanical behaviour of snow. Snow is, however, a highly complex material, and our understanding of its mechanical behavior is still very limited. Performing systematic mechanical experiments on snow is extremely difficult due to its fragile character. As an alternative, numerical experiments have been developed in the scope of this study to investigate the response of snow to mechanical loading. The obtained results have revealed that snow can fail in different modes. Depending on the level of applied loading, a dramatic collapse of the internal microstructure is observed. Moreover, consistent mechanical behavior was observed for different types of snow, including faceted crystals and rounded grains. The understanding of snow failure mechanisms resulting from this study thus represents a crucial ingredient for the development of large-scale snow avalanche simulations.

1. Introduction

Dry snow slab avalanches represent a severe natural hazard in mountainous regions and are very difficult to predict. They are released by a failure in a mechanically weaker layer of snow, underlying a cohesive slab (Schweizer et al., 2003). The weak layer consists of particular snow types, such as precipitation particles, faceted crystals, depth hoar, and surface hoar (Jamieson & Johnston, 1992), often characterized by very low strengths. On a slope, this layer of snow is loaded in combined shear and compression, the so-called mixed-mode loading, by the weight of the overlying snow and potential additional perturbations (skiers, animals, etc.). If the loading locally exceeds the weak layer strength, a failure occurs and can propagate along the slope as an anticrack (Gaume et al., 2017; Heierli et al., 2008). The loss of basal support results in an increase in tensile stresses within the slab and can eventually lead to a crown fracture and the release of a snow avalanche. Both the propagation of the anticrack in the weak layer and the release of the slab avalanche crucially depend on snow failure and collapse characteristics under mixed-mode loading (Gaume et al., 2018), which, however, remain poorly understood (Schweizer et al., 2016).

In the prefailure stage, the elastic properties of snow have been subject to numerous experimental investigations (Gerling et al., 2017; Mellor, 1975; Narita, 1980) and were shown to be controlled by density as well as microstructural anisotropy. Failure of snow is generally considered to be governed by the Mohr-Coulomb criterion (Chiaia et al., 2008; Fyffe & Zaiser, 2007; Gaume et al., 2014; McClung, 1977), where the shear strength

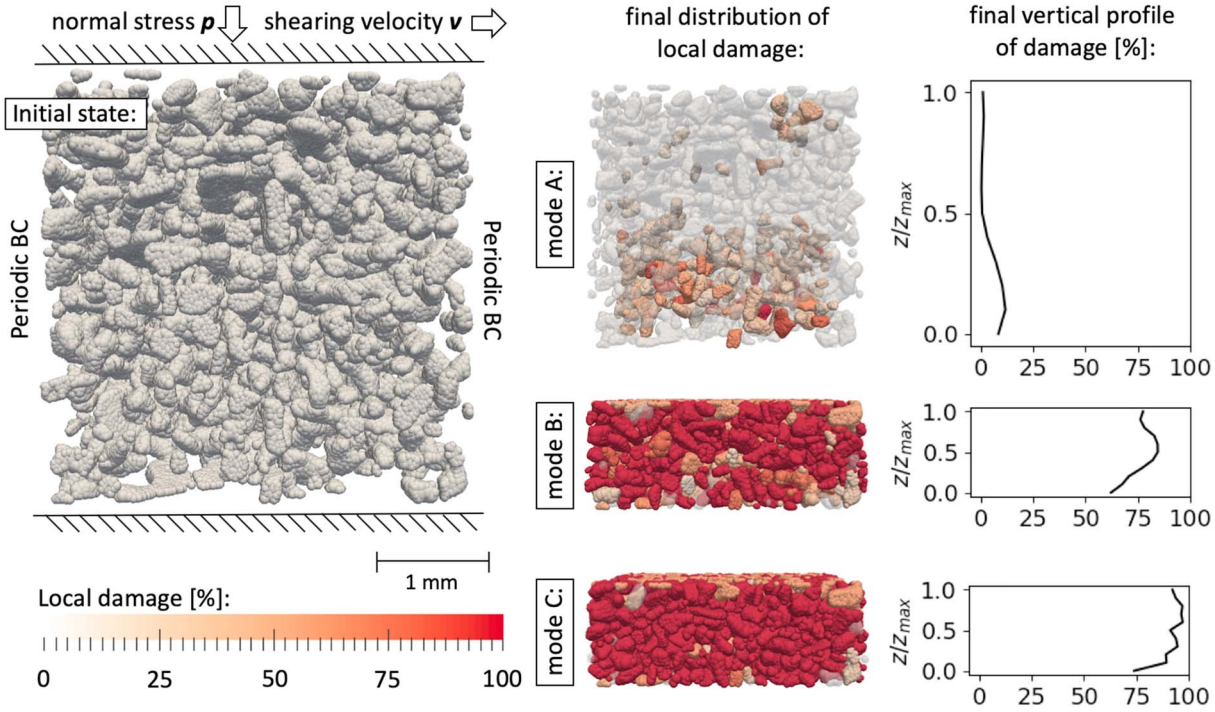

Figure 1. Snapshots of mixed-mode loading simulations, applied to sample s-RG1. Image on the left represents the intact sample, along with the boundary conditions. The three rows of images on the right represent the response of the sample under failure modes A ($p = 1$ kPa), B ($p = 4$ kPa), and C ($p = 9.5$ kPa). Grains with a local damage level below 10% (respectively above 10%) are represented as semitransparent (respectively with a red color scale according to the level of damage). The plots on the right represent averaged vertical damage profiles in the three failure modes.

increases linearly with the normal load. However, the application of this failure criterion to weak layers is questionable. Recent experimental campaigns have shown that weak layers feature closed failure envelopes (Chandel et al., 2014; Reiweger et al., 2015), which deviate from Mohr-Coulomb linear model at high levels of normal stresses and account for failure in pure compression. On the other hand, the postfailure mechanical behavior of snow, including strain softening and progressive transition toward residual stress remains largely unexplored (Fyffe & Zaiser, 2007; McClung, 1977). In addition, the mechanical response of weak layers is generally thought to be qualitatively different from that of other snow types, with a significant collapse at failure (Van Herwijnen et al., 2010). This normal collapse has been proven to have an important effect on the bending and fracture of the slab (Gaume et al., 2017). The conditions under which this collapse occurs, as well as its relation to failure and strain softening, remain open issues (Reuter & Schweizer, 2018).

The extremely low strength of weak layers and their sensitivity to environmental conditions render systematic experimental exploration difficult and complicate observation at the microscopic level. As an alternative to experiments, numerical approaches have been developed in the recent years to model snow mechanical response by accounting for microstructure (Gaume et al., 2017; Gerling et al., 2017; Hagenmuller et al., 2015; Srivastava et al., 2016; Wautier et al., 2015). These approaches enable the simulation of the macroscopic response of snow to mechanical loading from simple constitutive relations between snow particles at the microscopic scale. These approaches also offer the capacity to perform multiple loading simulations on the same sample, along with the perfect control over boundary conditions and access to all relevant descriptors.

The objective of the present study is to gain a deeper understanding of the mechanical response of snow to mixed-mode loading, using a microstructure-based numerical approach. Development of a specific discrete element model allows us to perform systematic large-strain shearing simulations on different snow types. We consider a regime in which snow deformation is dominated by intergranular damage and grain rearrangement and therefore model snow grains as unbreakable entities (Hagenmuller et al., 2015; Johnson & Hopkins, 2005). This regime is typical of the relatively high deformation rates involved in the release of snow avalanches, which are well above the rate of transition from ductile to brittle behavior of snow ($\dot{\gamma} > 10^{-4}$ s^{-1}, Narita, 1980). Accordingly, viscous effects at contacts and grain sintering are not considered in the model.

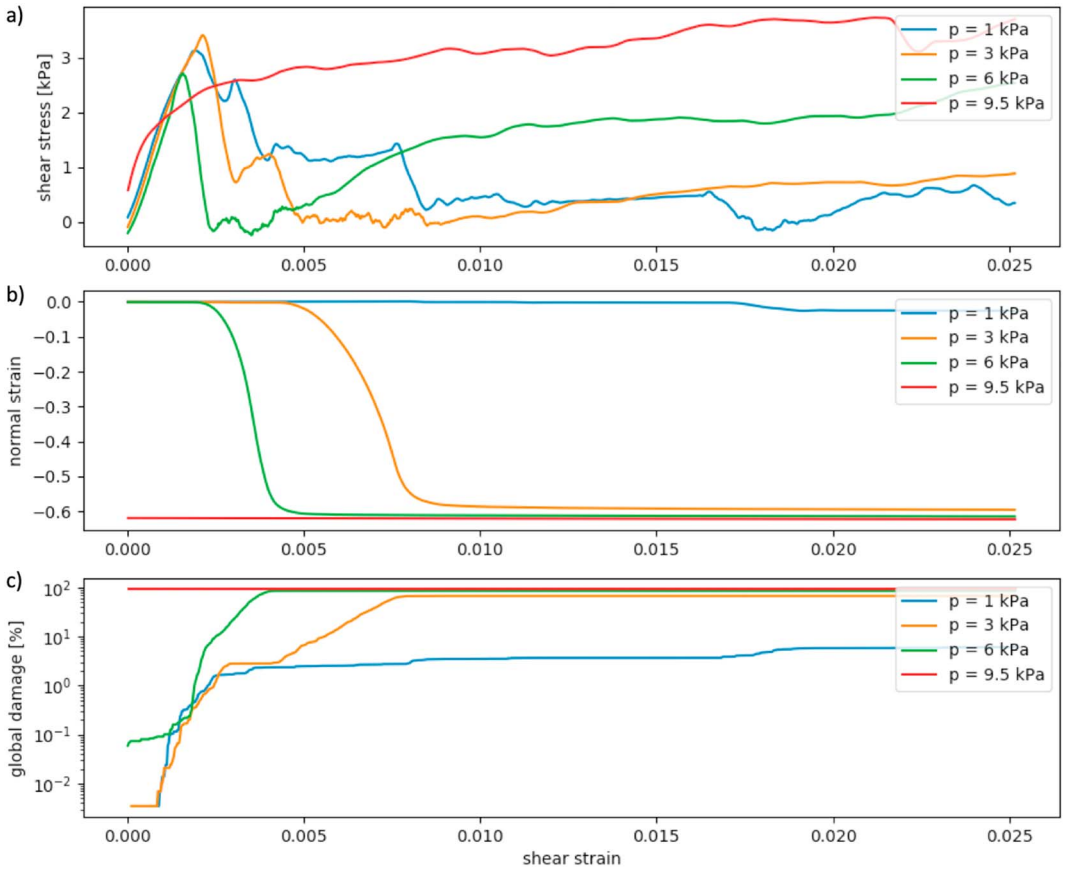

Figure 2. (a) Shear stress, (b) normal strain, and (c) global damage (in log scale) as a function of shear strain in snow sample s-RG1 during the mixed-mode loading simulations for four different values of normal stress: $p = 1$, $p = 3$, $p = 6$, and $p = 9.5$ kPa.

2. Methods

The present study exploits an original numerical approach, based on the discrete element method (DEM; Cundall & Strack, 1979), which has been developed in order to simulate the mechanical response of snow samples to external loading (Hagenmuller et al., 2015; Mede et al., 2018). The model takes X-ray microtomography images of snow as input information. First, the X-ray attenuation images are segmented into pore space and a continuous ice matrix (Hagenmuller et al., 2013). The ice structure itself is then segmented into individual grains by detecting potential weak points based on local geometrical criteria (Hagenmuller et al., 2014). For the sake of computational efficiency, the actual shape of every grain in DEM simulations is modeled by packing the volume of the grain with a set of overlapping spherical discrete elements (Mede et al., 2018). There is a trade-off between the grain approximation accuracy (and consequently the mechanical simulation accuracy) and the number of utilized spherical discrete elements (and consequently the numerical cost of the simulation). The optimal level of approximation was determined by a comprehensive sensitivity analysis of the macroscopic simulated response of a snow sample to compressive (Mede et al., 2018) as well as shear loading. These approximated grains are spatially arranged according to the initial microstructure. Grains are assumed to be unbreakable and are bonded by elastic brittle cohesion with the neighboring grains at the locations where the image has been segmented (Figure 1).

Considered snow samples are of cubical shape with a side length of approximately 5 mm. A rigid boundary condition is applied to the top and bottom faces, while a periodic boundary condition is applied to all four side faces (Figure 1). The samples are loaded by applying a constant shearing velocity $v = 1$ cm/s and constant normal stress p to the top surface, while keeping the bottom surface fixed. The normal stress is applied first with a ramp function. A time delay is then imposed before shearing is applied in order for existing kinetic energy within the sample to dissipate. It has been verified that the applied shear rate is low enough to ensure

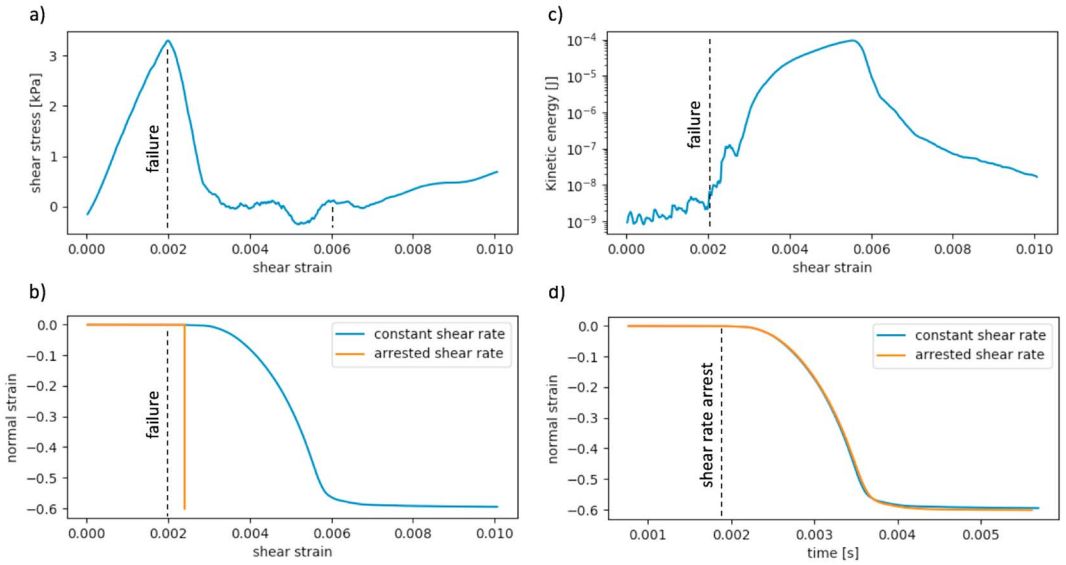

Figure 3. Response of the snow sample s-RG1 under mode B failure ($p = 4$ kPa): (a) shear stress with respect to shear strain; (b) normal strain with respect to shear strain; (c) kinetic energy with respect to shear strain; (d) normal strain with respect to time. In (c) and (d) the blue curve refers to the simulation where the shear rate was constant and the orange curve to the simulation where the shearing was stopped just after the stress peak (see text).

a quasi-static shearing regime, that is, that the stress-strain response is independent of v. Series of simulations were performed under different values of normal stress p, ranging from −5 to 10 kPa. The simulations were stopped once the shear strain reached the value $\gamma = 0.05$.

Three different snow samples (Mede, 2018) are considered in this study: sample s-RG1 (rounded grain snow, density= 250 kg/m^3), sample s-RG2 (rounded grain snow, density= 180 kg/m^3), and sample (faceted snow mixed with depth hoar, density= 180 kg/m^3). After the segmentation process, roughly 1,500 grains are identified in each sample. The choice of these samples allows us to compare the response obtained with the same snow type and different densities (samples s-RG1 and s-RG2), as well as the response obtained with the same density and different snow types (samples s-RG2 and s-FCDH).

The simulations were performed with DEM solver YADE (Šmilauer et al., 2010). The initial cohesive frictional grain contacts are modeled using a cohesion $C = 10^6$ Pa and Young's modulus $E = 10^8$ Pa. It has been verified that simulations are performed in the rigid grain limit (Cundall & Strack, 1979; Da Cruz et al., 2005). The noncohesive contacts created by grain rearrangement are modeled as elastic frictional with the same stiffness. Contact friction coefficient $\mu = 0.2$ was fixed according to typical ice values (Hagenmuller et al., 2015). A Cundall's nonviscous damping coefficient 0.02 was applied. Gravity is not taken into account as it has a negligible effect on the response of the samples compared to external loading. Lastly, the mass of each grain was derived from the original binary image. Due to volumetric errors induced by grain approximation (Mede et al., 2018), this results in an effective density typically increased by 15% compared to that of ice.

3. Results

Snapshots of snow sample s-RG1 submitted to mixed-mode loading under varying normal stresses are presented in Figure 1, and the macroscopic response of the sample is shown in Figure 2. Qualitatively, very similar response was observed for samples s-RG2 and s-FCDH. Local damage is defined for each grain as the ratio of broken cohesive bonds with the neighbouring grains, whereas the global damage represents the total ratio of broken cohesive bonds in the sample. In general, three qualitatively different modes of failure can be observed:

Failure mode A: at low normal stresses (for sample s-RG1, $p < 2$ kPa), a quasi-elastic shear stress build-up is followed by a peak (Figure 2a). The postpeak response is marked by progressive strain softening, which eventually stabilizes at a certain level of residual stress. Concurrently, the normal strain remains almost constant (Figure 2b), although a gradual compaction of the sample can be observed at the highest levels of normal

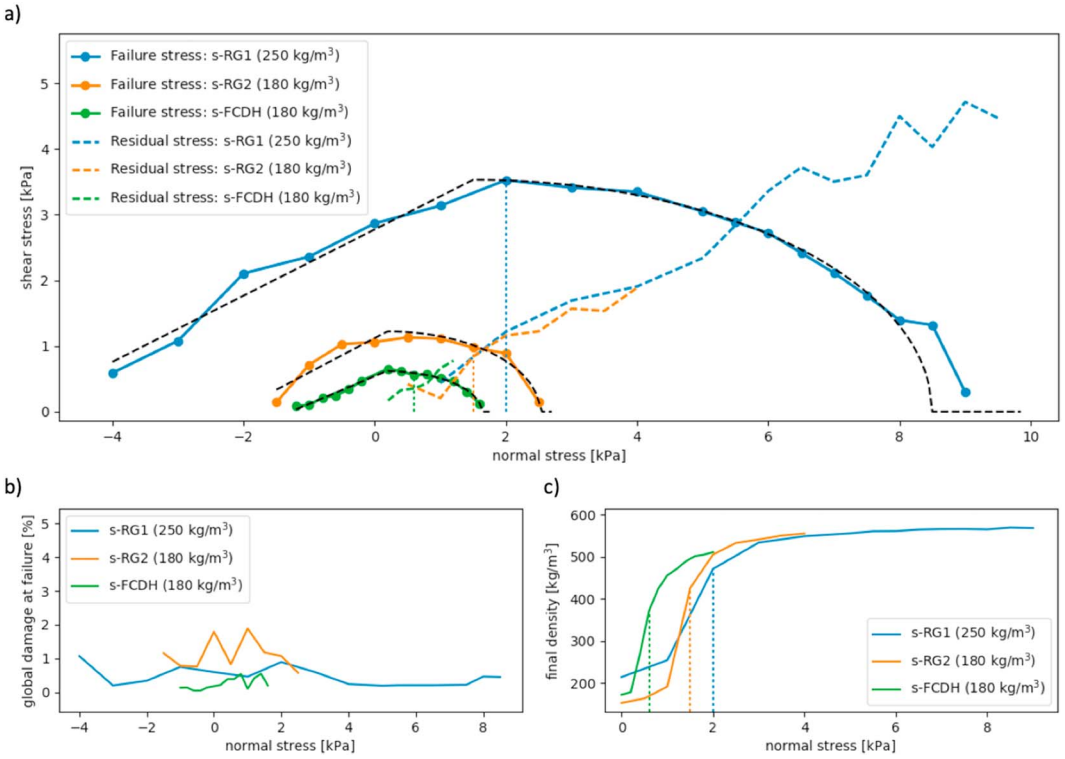

Figure 4. (a) Failure envelopes and residual stresses for the three different samples: s-RG1, s-RG2, and s-FCDH. Failure envelope parametrizations according to equation (1) are shown in dashed black lines. (b) Damage at failure as function of normal stress for the three samples. (c) Final sample density with respect to applied normal stress. The dotted vertical lines in images (a) and (c) mark the threshold normal stress, above which a collapse is observed (failure mode B).

stress in this mode. Failure initiation, marked by the stress peak, appears at a very low level of global damage (typically less than 2%; Figure 2c). The snow specimen fails along a narrow horizontal band, where all the damage is concentrated (Figure 1), while the rest of the specimen remains largely intact.

Failure mode B: at moderate normal stresses (for sample s-RG1, 2 kPa $\leq p <$ 9 kPa), the peak shear stress is followed by rapidly vanishing shear stress (Figure 2a). After this abrupt drop, the shear stress slowly increases and eventually stabilizes at the level of residual stress. The vanishing stress is accompanied by a dramatic vertical collapse (Figure 2b) and a burst of damage (Figure 2c). During the collapse the snow specimen is almost completely decomposed into a set of cohesionless grains (Figure 1). The onset of normal collapse appears to be progressively delayed with decreasing normal stress, consistently with a prolonged quasi-elastic phase.

Failure mode C: at high normal stresses (for sample s-RG1, $p \geq 9$ kPa), no quasi-elastic response is observed as the sample already fails and collapses during the normal loading phase (Figure 1), resulting in a high level of damage. Upon application of shearing, shear stress gradually increases to residual stress level, whereas the normal strain and damage level remain essentially constant (Figure 2).

The relation between failure and normal collapse in mode B was additionally explored by separate simulations (Figure 3), in which shear rate was stopped at different values of shear strain and the sample was let to evolve under constant normal stress. The shear rate was stopped with a ramp function to avoid inertial effects caused by the deceleration of the top surface. It was observed that if the shearing is stopped immediately after the shear stress peak, the normal collapse spontaneously develops in the same manner as if the shearing was kept constant (orange curves in Figures 3b and 3d). At failure the snow specimen enters a dynamic phase, where the collapse is driven by time rather than strain. A steep rise of the kinetic energy takes place immediately after the stress peak (Figure 3c), marking the start of a dynamical processes well before substantial normal strain can be observed.

Table 1
Parameter Values for the Failure Envelope Parametrization and Residual Friction Coefficients for the Three Tested Samples

	Failure envelope parameters			
Sample	p_0	τ_T	p_T	Residual friction
s-RG1	7.00	3.53	1.49	0.49
s-RG2	2.33	1.22	0.19	0.46
s-FCDH	1.45	0.61	0.17	0.59

Figure 4 summarizes the response of the three simulated snow samples with respect to the level of applied normal stress. Failure envelopes (Figure 4a) are defined based on the stress values recorded at the initial shear stress peak. The obtained failure envelopes display similar closed shapes for the three samples, with shear failure stress diminishing to zero at sufficiently low or sufficiently high normal stress. The decrease of failure shear stress at sufficiently large normal stress is a consequence of sample collapse. Note that the maximum of the failure envelopes roughly coincides with the onset of failure mode B and sample collapse (marked by the dotted vertical lines on Figure 4a). The following linear-elliptic parametrization was found to provide a good fit for the failure envelopes (Figure 4a):

$$\tau = \begin{cases} \frac{\tau_T}{p_0} p + \left(\tau_T - \frac{\tau_T p_T}{p_0}\right), & \text{if } \left(p_T - p_0 \le p \le p_T\right) \\ \sqrt{\tau_T^2 - \frac{\tau_T^2}{p_0^2}\left(p - p_T\right)^2}, & \text{if } \left(p_T < p \le p_T + p_0\right) \\ 0, & \text{otherwise,} \end{cases} \tag{1}$$

where τ is the shear stress; p is the normal stress; and p_0, τ_T, and p_T are three parameters. Least squares fitting was used to obtain the value of the parameters for each sample (Table 1).

For the three samples, the residual shear stresses appear to follow a common linear trend as a function of normal stress, consistent with a Mohr-Coulomb relation, as expected for a cohesionless granular material. Obtained values of the residual friction coefficients for the three samples vary between 0.49 and 0.59 (Table 1).

Figure 4b displays the global damage of the three samples at the point of failure. It must be noted that the results are displayed only for failure modes A and B, since failure in mode C is already triggered before shearing is applied. Noteworthy are the extremely low levels of global damage necessary to trigger failure, which remain below 2% for all three samples through the entire range of normal stresses. It also appears that the level of damage at failure is roughly constant throughout the normal stress domain.

Figure 4c exhibits the final sample density with respect to the applied normal stress. At low normal stresses, in the absence of collapse, the density of the samples is not substantially changed during shearing and the final density is heavily influenced by the initial microstructure. As the normal stress increases, the final density increases rapidly. Above the collapse threshold stress, the curve slopes start diminishing and all three curves seem to converge toward a unique value independent of normal stress, consistent with the decomposition of the initial microstructure into a cohesionless assembly of grains.

4. Discussion and Conclusions

DEM simulations conducted in this study offer a unique insight into the failure of snow under mixed-mode shear and normal loading. Three distinct failure modes were identified: a shear failure without normal collapse at low levels of normal stress (mode A); a normal collapse, initiated by shear that takes place at moderate levels of normal stress (mode B); and a normal failure and collapse that take place at high levels of normal stress (mode C). In mode B, sample failure is triggered by extremely low levels of global damage due to combined shear and normal loading. The normal collapse is accompanied by a burst of global damage and nearly completely disintegrates the sample. This normal collapse was shown to be a dynamic event that, once initiated, spontaneously develops independently of shearing. In this mode, apparent postpeak softening of the stress is intimately coupled to sample collapse. Shear stress temporarily drops to zero and the process is time rather than strain controlled. In other words, the postfailure behavior in case of collapse should be seen as the response to a boundary value problem rather than an intrinsic constitutive feature of the material. This

may have important consequences for the modeling of collapse wave propagation in slab avalanche release (Gaume et al., 2018).

A consistent macroscopic response was observed for the three tested types of snow, one of which is typical of persistent weak layers (faceted snow). The fact that identical failure modes are observed for all three samples appears to contradict the idea that the mechanical response of weak layers qualitatively differs from other snow types. In particular, according to the performed numerical experiments, the normal collapse, which has hitherto been associated with weak layers (Van Herwijnen et al., 2010), seems to be a general failure characteristic of snow, provided that normal stress is sufficient to activate failure mode B or C.

Due to their collapsible character, the three tested snow samples all feature qualitatively similar, closed failure envelopes. Nevertheless, quantitative discrepancies between the three simulated failure envelopes are observed. On one hand, the differences observed between samples s-RG1 and s-RG2, which correspond to the same snow type with different densities, confirm the well established positive correlation between the snow density and its ultimate strength (McClung, 1977; Narita, 1980). On the other hand, the differences between the samples s-RG2 and s-FCDH, which have the same density but consist of different snow types, suggests a nonnegligible effect of other microstructural characteristics of snow on its ultimate strength. This result is consistent with various experimental investigations, indicating that microstructure plays an important role in determining the mechanical properties of snow (Keeler & Weeks, 1968; Narita, 1980).

Results showed that an extremely low level of damage is sufficient to trigger sample failure, which underlines the extremely fragile character of snow. Furthermore, this damage level seems to be completely independent of the applied normal stress. Note that although small, the sample size considered in this study has been shown to result in a representative mechanical response in the case of simulated large-strain compression (Hagenmuller et al., 2015) on samples s-RG1 and s-FCDH. Additionally, the size of these two samples was proven sufficient to estimate the minimum cut density (Hagenmuller et al., 2014), which is related to the minimal damage needed to break the sample. We can thus argue that this sample size is also sufficient to monitor representative damage evolution under mixed-mode loading.

As a preliminary validation of the model, we can note a good qualitative agreement with the currently available experimental results in several respects: (1) Experimentally obtained weak layer failure envelopes and typical strength values (in the range 1–10 kPa; Chandel et al., 2014; Reiweger et al., 2015) appear very similar to those presented in this paper. (2) The volumetric collapse at failure observed in this study is well documented in weak layers by in situ (Van Herwijnen et al., 2010) as well as laboratory measurements (Reiweger & Schweizer, 2013). (3) The derived values of residual friction coefficients are in agreement with those obtained from field tests (between 0.5 and 0.7; Van Herwijnen & Heierli, 2009). Finally, the extremely low levels of damage observed at peak strength are also consistent with results obtained by Hagenmuller et al. (2014), using tensile finite-element simulations on X-ray microtomography snow images. Hence, the developed numerical model indeed appears to represent a useful tool to investigate failure and post-failure behaviour of snow, including weak layers. Direct quantitative comparisons with experiments are currently not possible since a detailed characterization of the snow microstructure, needed as input for the developed model, is not supplied with available experimental results.

Recent advances in the constitutive modeling of snow and the use of Material Point Method showcase promising perspectives for the simulation of snow avalanche release (Gaume et al., 2018). The results obtained with the DEM approach proposed here clearly confirm the assumption of closed failure envelopes made in the latter study. In the future, exciting progress in the multiscale problem of simulating large-scale avalanches from the microstructure is expected by better connecting the continuum mechanics models to material parameters derived from X-ray tomography images.

Acknowledgments
All data for the present work are available at: https://osf.io/x59fh/. We would like to thank Mohamed Naaim for fruitful discussions and support. This project is funded by Labex TEC21 (Investissements d'Avenir, grant agreement ANR-11-LABX-0030). CNRM / CEN and Irstea UR ETGR are part of Labex OSUG@2020 (Investisssments d'Avenir, grant agreement ANR-10-LABX-0056). We thank Henning Löwe and an anonymous reviewer for their constructive comments.

References

Chandel, C., Mahajan, P., Srivastava, P. K., & Kumar, V. (2014). The behaviour of snow under the effect of combined compressive and shear loading. *Current Science*, *107*, 888–894.

Chiaia, B. M., Cornetti, P., & Frigo, B. (2008). Triggering of dry snow slab avalanches: stress versus fracture mechanical approach. *Cold Regions Science and Technology*, *53*(2), 170–178.

Cundall, P. A., & Strack, O. D. L. (1979). Discrete numerical model for granular assemblies. *Geotechnique*, *29*(1), 47–65.

Da Cruz, F., Emam, S., Prochnow, M., Roux, J.-N., & Chevoir, F. (2005). Rheophysics of dense granular materials: Discrete simulation of plane shear flows. *Physical Review E*, *72*(2), 021309.

Fyffe, B., & Zaiser, M. (2007). Interplay of basal shear fracture and slab rupture in slab avalanche release. *Cold Regions Science and Technology*, *49*(1), 26–38.

Gaume, J., Gast, T., Teran, J., van Herwijnen, A., & Jiang, C. (2018). Dynamic anticrack propagation in snow. *Nature Communications*, *9*(1), 3047.
Gaume, J., Löwe, H., Tan, S., & Tsang, L. (2017). Scaling laws for the mechanics of loose and cohesive granular materials based on Baxter's sticky hard spheres. *Physical Review E*, *96*(3), 032914.
Gaume, J., Schweizer, J., Herwijnen, A., Chambon, G., Reuter, B., Eckert, N., & Naaim, M. (2014). Evaluation of slope stability with respect to snowpack spatial variability. *Journal of Geophysical Research: Earth Surface*, *119*, 1783–1799. https://doi.org/10.1002/2014JF003193
Gaume, J., van Herwijnen, A., Chambon, G., Wever, N., & Schweizer, J. (2017). Snow fracture in relation to slab avalanche release: Critical state for the onset of crack propagation. *The Cryosphere*, *11*(1), 217–228.
Gerling, B., Löwe, H., & van Herwijnen, A. (2017). Measuring the elastic modulus of snow. *Geophysical Research Letters*, *44*, 11–088. https://doi.org/10.1002/2017GL075110
Hagenmuller, P., Calonne, N., Chambon, G., Flin, F., Geindreau, C., & Naaim, M. (2014). Characterization of the snow microstructural bonding system through the minimum cut density. *Cold Regions Science and Technology*, *108*, 72–79.
Hagenmuller, P., Chambon, G., Flin, F., Morin, S., & Naaim, M. (2014). Snow as a granular material: Assessment of a new grain segmentation algorithm. *Granular Matter*, *16*(4), 421–432.
Hagenmuller, P., Chambon, G., Lesaffre, B., Flin, F., & Naaim, M. (2013). Energy-based binary segmentation of snow microtomographic images. *Journal of Glaciology*, *59*(217), 859–873.
Hagenmuller, P., Chambon, G., & Naaim, M. (2015). Microstructure-based modeling of snow mechanics: A discrete element approach. *Cryosphere*, *9*(5), 1969–1982.
Hagenmuller, P., Theile, T. C., & Schneebeli, M. (2014). Numerical simulation of microstructural damage and tensile strength of snow. *Geophysical Research Letters*, *41*, 86–89. https://doi.org/10.1002/2013GL058078
Heierli, J., Gumbsch, P., & Zaiser, M. (2008). Anticrack nucleation as triggering mechanism for snow slab avalanches. *Science*, *321*(5886), 240–243.
Jamieson, J. B., & Johnston, C. D. (1992). Snowpack characteristics associated with avalanche accidents. *Canadian Geotechnical Journal*, *29*(5), 862–866.
Johnson, J. B., & Hopkins, M. A. (2005). Identifying microstructural deformation mechanisms in snow using discrete-element modeling. *Journal of Glaciology*, *51*(174), 432–442.
Keeler, C. M., & Weeks, W. F. (1968). Investigations into the mechanical properties of alpine snow-packs. *Journal of Glaciology*, *7*(50), 253–271.
McClung, D. M. (1977). Direct simple shear tests on snow and their relation to slab avalanche formation. *Journal of Glaciology*, *19*(81), 101–109.
Mede, T. (2018). Snow samples. Retrieved from https://osf.io/x59fh/
Mede, T., Chambon, G., Hagenmuller, P., & Nicot, F. (2018). A medial axis based method for irregular grain shape representation in dem simulations. *Granular Matter*, *20*(1), 16.
Mellor, M. (1975). *A review of basic snow mechanics*. In *Symposium at Grindelwald 1974 – Snow Mechanics, IAHS Publ*. (Vol. 114, pp. 251–291).
Narita, H. (1980). Mechanical behaviour and structure of snow under uniaxial tensile stress. *Journal of Glaciology*, *26*(94), 275–282.
Reiweger, I., Gaume, J., & Schweizer, J. (2015). A new mixed-mode failure criterion for weak snowpack layers. *Geophysical Research Letters*, *42*, 1427–1432. https://doi.org/10.1002/2014GL062780
Reiweger, I., & Schweizer, J. (2013). Weak layer fracture: Facets and depth. *Cryosphere*, *7*(5), 1447–1453.
Reuter, B., & Schweizer, J. (2018). Describing snow instability by failure initiation, crack propagation and slab tensile support. *Geophysical Research Letters*, *45*, 7019–7027. https://doi.org/10.1029/2018GL078069
Šmilauer, V., Catalano, E., Chareyre, B., Dorofeenko, S., Duriez, J., Gladky, A., et al. (2010). *Yade reference documentation*. In V. Šmilauer (Ed.), Yade Documentation (Vol. 474). Retrieved from http://yadedem.org/doc/
Schweizer, J., Jamieson, J. B., & Schneebeli, M. (2003). Snow avalanche formation. *Reviews of Geophysics*, *41*(4), 1016. https://doi.org/10.1029/2002RG000123
Schweizer, J., Reuter, B., van Herwijnen, A., & Gaume, J. (2016). Avalanche release 101. In *Proceedings ISSW* (pp. 1–11). Breckenridge, CO, USA.
Srivastava, P. K, Chandel, C., Mahajan, P., & Pankaj, P. (2016). Prediction of anisotropic elastic properties of snow from its microstructure. *Cold Regions Science and Technology*, *125*, 85–100.
Van Herwijnen, A., & Heierli, J. (2009). Measurement of crack-face friction in collapsed weak snow layers. *Geophysical Research Letters*, *36*, L23502. https://doi.org/10.1029/2009GL040389
Van Herwijnen, A., Schweizer, J., & Heierli, J. (2010). Measurement of the deformation field associated with fracture propagation in weak snowpack layers. *Journal of Geophysical Research*, *115*, F03042. https://doi.org/10.1029/2009JF001515
Wautier, A., Geindreau, C., & Flin, F. (2015). Linking snow microstructure to its macroscopic elastic stiffness tensor: A numerical homogenization method and its application to 3-D images from x-ray tomography. *Geophysical Research Letters*, *42*, 8031–8041. https://doi.org/10.1002/2015GL065227